35th AIAA Fluid Dynamics Conference and Exhibit
6 - 9 June 2005, Toronto, Ontario Canada

AIAA 2005-4912

A Comparison of Two POD Methods for Airfoil Design Optimization

Xiaodan Cai*
Thaerocomp Technical Corporation, P.O. Box 1527, Stony Brook, NY 11790

Foluso Ladeinde†
Department of Mechanical Engineering, SUNY at Stony Brook, Stony Brook, NY 11794-2300

Proper-orthogonal-decomposition (POD) methods have recently been developed for the design of airframe components. In this paper, two POD-based approaches have been studied: the Gappy POD reconstruction procedure (Ref. 6) and the gradient approach (Ref. 7). Both methods do not require a projection onto the CFD governing equations, but are, instead, a collection of flow snapshots that covers the parameter ranges of interest. Their performance on the inverse design of various airfoil shapes such as Korn, NACA63212, HQ2010, and GOE117 airfoils has been compared and evaluated. Our studies show that, while both methods are efficient and accurate once appropriate flow snapshots have been collected, the gradient-based method is generally more accurate..

Nomenclature

$\boldsymbol{U}$	=	flow solutions around an airfoil
$\boldsymbol{\psi}$	=	POD basis vector
$\boldsymbol{K}$	=	POD autocorrelation tensor
$\boldsymbol{R}$	=	Reduced POD autocorrelation tensor
$\boldsymbol{X}$	=	spatial location
N	=	number of snapshots
M	=	reduced number of POD modes
β	=	coefficient of POD mode
J	=	cost function
P	=	pressure
P^*	=	target pressure
V	=	extended design variable in Gappy POD
V^*	=	target design variable in Gappy POD
$\hat{V}$	=	Gappy data
Ma	=	Mach number
α	=	attack angle
m	=	missing data index matrix
c	=	chord length
b	=	Hicks-Henne function
t_1	=	the first control parameter in Hicks-Henne function
t_2	=	the second control parameter in Hicks-Henne function

I. Introduction

AERODYNAMIC shape optimization is receiving attention in the aerospace industry as a useful tool for the design of airframe components. The analysis usually involves a gradient-based optimizer and an adjoint solver, which can then be coupled to a computational fluid dynamics (CFD) solver that provides the required gradients.

*Senior Research Engineer, AIAA Member.
† Associate Professor, Associate Fellow, AIAA.

Significant progress has been reported on the application of this approach to realistic design of complex geometries and viscous flows (Jameson, 2004; Lund et al., 2001). However, the use of this adjoint-solver approach for situations involving multiple disciplines and a large number of design constraints has been somewhat limited. The fundamental reason for this might be related to the fact that the adjoint equations, boundary conditions, and gradient calculation formulae are cost function-dependent, and therefore need to be re-derived every time the cost function changes. Moreover, it is not possible to treat arbitrary forms of the cost functions, thus limiting the applicability of this procedure. In this work, alternative approaches for aerodynamic design of wings based on proper-orthogonal-decomposition (POD) method have been evaluated by the application to inverse design of a series of airfoil shapes.

POD has been used in reduced-order methods for multi-disciplinary design environments, where aerodynamics, structures, and realistic descriptions of aircraft/spacecraft models are included (Romanowski, 1996; Glauser et al., 2004; Lucia et al., 2004). The work by Bui-Thanh et al (2003) and LeGresley and Alonso (2000) have demonstrated that the POD method could also be used as a low-cost, low-order approximation for aerodynamic shape optimization. These methods do not require a projection onto the CFD governing equations, but are, instead, a collection of flow snapshots that covers the parameter ranges of interest. The method proposed by Bui-Thanh et al (2003) was based on the Gappy POD reconstruction procedure (Everson and Sirovich, 1995), while that used by LeGresley and Alonso (2000) was based on the gradient approach to cost function optimization. In both cases, conventional computational fluid dynamics (CFD) methods were used to generate the data ensemble (snapshots) for the airfoil inverse design problem. The POD process computes a set of optimal eigenfunctions from these snapshots. The two methods differ from each other in the way the cost function is evaluated and the optimal solutions are approached. In the current paper, the effectiveness and accuracy of the two methods discussed above have been evaluated as a function of the size of the snapshots, the size of reduced POD modes, and the values of the variables for geometry optimization.

II. Proper Orthogonal Decomposition (POD)

The POD procedure used here relies on the Karhunen-Loève expansion for the data ensembles which span a range of airfoil geometries. The construction of the basis for the POD procedure considered is summarized below, wherein a snapshot of the flow field around an airfoil is denoted by $U(\mathbf{x})$. If the airfoil geometry is indexed by n, the ensemble is denoted by $\left\{\mathbf{U}^n\right\}$, where $1 \le n \le N$, and N represents the number of geometries in the ensemble. The POD basis vector, $\boldsymbol{\psi}$, is chosen in an optimal way in the sense that the average error,

$$\varepsilon = \left\langle \left\| \mathbf{U} - \sum_{n=1}^{M} a_n \boldsymbol{\psi}_n \right\|_2 \right\rangle, \qquad (1)$$

is minimal for all M ($1 \le M \le N$). Here $\|\cdot\|_2$ denotes the usual L_2 norm and $\langle\cdot\rangle$ denotes the average over the ensemble. It has been shown (Ref. 9) that the POD basis vector, $\boldsymbol{\psi}$, satisfies the eigen-value problem

$$\mathbf{K}\boldsymbol{\psi}_n = \lambda \boldsymbol{\psi}_n, \qquad (2)$$

where the matrix operator $\mathbf{K}$ is the autocorrelation tensor given by

$$\mathrm{K}_{ij} = \frac{1}{N}\sum_{n=1}^{N} U^n(\mathbf{x}_i) U^n(\mathbf{x}_j). \qquad (3)$$

Since the dimension of $\mathbf{K}$ is the mesh size (N_c) of the flow field, which could be millions for realistic calculations, it is usually inefficient to solve Equation (2) directly. An alternative method to determine the POD basis functions proposed by Sirovich (Ref. 9) represents the functions as a linear combination of the snapshots, as follows:

$$\psi_n(\mathbf{x}) = \sum_{i=1}^{N} \beta_i^n U^i(\mathbf{x}), \qquad (4)$$

where the coefficients β^n satisfy the eigen-value equation

$$\mathbf{R}\boldsymbol{\beta}^n = \lambda \boldsymbol{\beta}^n. \qquad (5)$$

Here, the correlation matrix is

$$R_{kl}=\frac{1}{N_c}\sum_{i=1}^{N_c}U^k(x_i)U^l(x_i)\,, \qquad (6)$$

and its dimension is of the size of the snapshots, which is much smaller than the grid size for the flow fields. Once these basis functions have been obtained, we can expand the flow solution about an arbitrary airfoil shape (δ), i.e.,

$$U^\delta \approx \sum_{j=1}^{n} a_j^\delta \psi_j\,. \qquad (7)$$

The accuracy of the expansion depends on the scope of the database and the number of POD eigen-modes (n). The purpose of this paper is to investigate the effects of these two factors on the performance of two previously-reported POD-based inverse design procedures which are described below, within the framework of airfoil shape design.

III. Inverse Design

The procedure we have used for inverse design is summarized in this section. Given a target pressure distribution $\mathbf{P}^*$, the inverse design problem is to find an optimal airfoil shape whose surface pressure distribution $\mathbf{P}$ minimizes the cost function

$$J=\left\|\mathbf{P}^*-\mathbf{P}\right\|_2\,. \qquad (8)$$

As mentioned above, the performance of two POD-based inverse design procedures is evaluated in this paper. One is based on the Gappy procedure developed by Bui-Thanh et al (2003). The key point of this method is that, rather than containing only flow variables, the snapshot is augmented to also contain airfoil coordinates. The minimal solution of a cost function

$$J=\left\|\mathbf{V}^*-\mathbf{V}\right\|_2 \qquad (9)$$

is sought, where the new target vector $\mathbf{V}^*$ contains a surface pressure distribution $\mathbf{P}^*$ and the corresponding airfoil coordinates $\mathbf{C}^*$. As the target pressure distribution $\mathbf{P}^*$ is known to the designer, the new target vector $\mathbf{V}^*$ then contains both known and unknown components. Everson and Sirovich (1995) have developed a POD procedure to reconstruct the missing (Gappy) data by assuming that

$$\mathbf{V}^* \approx \overline{\mathbf{V}}=\sum_{n=1}^{M}\overline{a}_n\boldsymbol{\psi}_n\,. \qquad (10)$$

The error

$$E=\int_{s[\overline{\mathbf{V}}]}\left[\hat{\mathbf{V}}(\mathbf{x})-\sum_{n=1}^{M}\overline{a}_n\boldsymbol{\psi}_n\right]^2 d\mathbf{x}\,, \qquad (11)$$

is minimized over the support $s\left[\hat{\mathbf{V}}\right]$ of $\hat{\mathbf{V}}$. The vector $\hat{\mathbf{V}}$ is defined as

$$\hat{\mathbf{V}}(\mathbf{x})=m(\mathbf{x})\mathbf{V}^*(\mathbf{x})\,, \qquad (12)$$

where m is zero on the missing data, and unity elsewhere. The minimization of E leads to following equations:

$$\mathbf{M}\cdot\overline{\mathbf{a}}=\mathbf{f}\,, \qquad (13)$$

$$M_{kn}=\left(\boldsymbol{\psi}_k,\boldsymbol{\psi}_n\right)_{s[\overline{\mathbf{V}}]}, \qquad (13a)$$

$$f_k=\left(\mathbf{V},\boldsymbol{\psi}_k\right)_{s[\overline{\mathbf{V}}]}, \qquad (13b)$$

where the inner product is over the support $s\left[\hat{\mathbf{V}}\right]$.

The second POD-based inverse design procedure investigated in this paper is the gradient optimization approach of LeGresley and Alonso (2000). For this approach, the cost function is as defined in Eq. (8), and $\mathbf{P}$ is represented by the POD modes, i.e.,

$$\mathbf{P}=\sum_i b_i\boldsymbol{\psi}_i\,. \qquad (14)$$

The POD coefficients b_i are functions of the design variables, which are chosen as the amplitudes of bumps that are added to the basic airfoil geometries. In the current work, the bump functions are a series of Hicks-Henne functions (Ref. 10):

$$b(x) = \left\{ \sin\left[\pi x^{\log 0.5/\log(t_1)} \right] \right\}^{t_2}, \quad 0 \le x \le 1. \qquad (15)$$

In this paper, the gradients of the cost function with respect to the design variables have been obtained by finite-differencing of the POD coefficients.

.

IV. Results

First, our implementation of the Gappy POD-reconstruction procedure is tested on the NACA0012 airfoils. Note that the same calculations have been reported by Bui-Thanh et al (2003) and are carried out here solely for the purpose of validating our implementation. The database is generated by varying the Mach number and attack angle of the free-stream flows. The Mach numbers used are M_a=0.75, 0.775, 0.800, 0.825, 0.85, while the attack angles are α=0°, 0.25°, 0.50°, 0.75°, 1.00°, and 1.25°. Hence the total number of snapshots in the ensemble is 30. The Gappy data (incomplete flow quantities) consists of only the surface pressure data for M_a=0.75 and α= 0.75°. The pressures in the outer field are assumed to be unknowns. The goal is to reconstruct the full pressure field using the above Gappy POD method. Such a test is not only useful in validating the Gappy POD approach for optimal design of airfoil shapes, but also useful in realistic situations where partial experimental data is available and the entire flowfield could be reconstructed using the Gappy POD method. Figures 1(a) through 1(c) compare the reconstructed pressure contours with the original CFD solution. As expected, the larger the number of the eigen-modes used, the more accurate the reconstruction. Therefore, with only the surface pressure data available, the complete pressure field can be determined very accurately by the Gappy method.

For inverse design, the snapshots were generated for RAE2822 airfoil to which a series of Hicks-Henne bump functions is added. First, 14 bump functions were added to the basic RAE2822 airfoil, where 7 each were distributed uniformly on the upper and lower surfaces, respectively, and are shown in Figure 2 with dashed lines. Flow solutions for the original airfoil plus the 14 modified airfoils are computed using the commercial software AEROFLO (Ref. 11), which is a high-order CFD code for multi-disciplinary applications. With the ensemble of the generated flow solutions, the POD basis with a complete set of modes is generated and used for the following inverse design problems.

The surface pressure distribution for the Korn airfoil, whose geometry is also shown in Figure 2 with solid lines, is specified as the design target. It can be seen in this figure that, while the Korn airfoil shares some similarities with the RAE 2822-based snapshot set, its camber and thickness distributions are quite different. This example thus represents a challenge for both POD-based optimal methods. Figures 3(a) and 3(b) compare the exact Korn airfoil geometry and the target pressure to the POD design results using Gappy POD method (long-dashed lines) and cost-function optimization method (short-dashed lines). It can be seen that the POD design results are close to those of the target except in a few regions. Also, the gradient cost-function optimization POD approach produces better results than the Gappy POD method. However, in the lower-side trailing tips and the upper-side leading edge regions, we see that both methods produce significant errors relative to the target shape, implying the need for improvement.

One way to improve inverse design is to increase the richness of the subspace spanned by the POD basis vectors. This can be achieved by increasing the number of snapshots in the ensemble. To test this, four more bumps (t_1=0.05, 0.10, 0.20, 0.40 in the Hicks-Henne functions) have been added on the top part of the RAE2822 airfoils, and one more bump (t_1=0.925) added on the bottom part of the airfoil. Figures 3(c) and 3(d) compare the exact Korn airfoil geometry and the target pressure to the POD design results using the Gappy POD method (long, dashed lines) and cost-function optimization method (short, dashed lines) with the extended snapshot database. Improved results are evident for both POD methods. Note that the gradient-based cost function optimization method almost recovers the target airfoil shapes and the surface pressure distributions. The r.m.s. errors of the computed y-coordinates and the surface pressures between the targets and the designed values have been listed in Table 1, which quantitatively supports the above observations for the Korn airfoil. The r.m.s. errors are defined here as

$$\varepsilon_y = \sqrt{\sum_i \left(y_i - y_i^T\right)^2} \,/\, y_{\max}^T, \qquad \varepsilon_p = \sqrt{\sum_i \left(p_i - p_i^T\right)^2} \,/\, p_{\max}^T,$$

where $y_{\max}^T$ are the maximum airfoil thickness of the target airfoil, and $p_{\max}^T$ are the maximum surface pressure of the target airfoil.

		15		20		Deviation From Baseline	
		ε_y	ε_p	ε_y	ε_p	ε_y	ε_p
Korn	GAPPY	4.08×10^{-2}	1.21×10^{-2}	2.82×10^{-2}	8.94×10^{-3}	7.47×10^{-2}	1.62×10^{-2}
	GRAD	3.33×10^{-2}	1.31×10^{-2}	1.48×10^{-2}	9.53×10^{-3}		
NACA63212	GAPPY	3.00×10^{-2}	1.35×10^{-2}	3.29×10^{-2}	1.25×10^{-2}	6.23×10^{-2}	2.16×10^{-2}
	GRAD	2.63×10^{-2}	1.48×10^{-2}	2.93×10^{-2}	1.37×10^{-2}		
HQ2010	GAPPY	3.72×10^{-2}	1.39×10^{-2}	4.50×10^{-2}	1.19×10^{-2}	1.47×10^{-1}	2.88×10^{-2}
	GRAD	3.62×10^{-2}	1.50×10^{-2}	3.90×10^{-2}	1.33×10^{-2}		
GOE117	GAPPY	5.61×10^{-2}	1.44×10^{-2}	5.69×10^{-2}	1.34×10^{-2}	2.37×10^{-1}	4.38×10^{-2}
	GRAD	4.57×10^{-2}	1.45×10^{-2}	4.38×10^{-2}	1.39×10^{-2}		

Table 1: The r.m.s. errors of the computed y-coordinates and the surface pressures.

Using the same ensemble of snapshots as in the previous case, three more target airfoils, namely, NACA63212, HQ2010, and GOE117 have been tested. To quantify the deviations of the target airfoils away from the baseline airfoils, the rms errors of the computed y-coordinates and the surface pressures between the target airfoils and the baseline RAE2822 airfoils have also been calculated in Columns 7 and 8 of Table 1. It can be seen from this table that, for the surface pressures, the Korn airfoil is the closest to the baseline airfoil, and the GOE117 airfoil differs the most from the baseline airfoil. The design errors for GOE117 are also the most significant, which shows the importance of the choice of the flow snapshots, as pointed out in Refs. (6) and (7).

The designed airfoil geometries and surface pressures from both database sets with 15 and 20 snapshots have also been presented in Figure 4 (NACA63212), Figure 5 (HQ2010) and Figure 6 (GOE117), respectively. From these results, it is consistently shown that with the sample ensembles, the gradient-based POD optimization method out-performs (short-dash lines in the figures) the Gappy POD method for shape optimizations, even though the gradient-based POD method shows larger errors for the target surface pressure. It is pointed out that the gradient-based POD optimization method enables a different definition of cost function, relative to Equation (8). This could be beneficial to the optimal design of a specific airfoil. On the other hand, we found that, except for the Korn airfoil, the ensemble with 20 snapshots does not improve the results, compared to the ensemble with 15 snapshots. This further demonstrates the importance of the choice of the flow snapshots.

V. Conclusion

With the same ensembles, both the Gappy POD method and the gradient-based POD optimization method have been used for inverse design of Korn, NACA63212, HQ2010, and GOE117 airfoils. We have shown that the two optimization methods are efficient and accurate once appropriate flow snapshots have been collected. With the same ensembles, the gradient-based POD optimization method appears to give better results.

Acknowledgments

This work was supported from an Air Force SBIR Phase II contract, with Dr. Datta Gaitonde as Technical Monitor. Mr. Jesse Fite generated the database for the flows around the RAE2822 airfoil.

References

[1] Jameson, A. "Advances in Aerodynamic Shape Optimization," International Conference on CFD, Toronto, Canada, 12-16 July, 2004.
[2]Lund, E., Moller, H., and Jakobsen, L.A., "Shape Design Optimization of Steady Fluid-Structure Interaction Problems with Large Displacements," AIAA 2001-1624, 2001.
[3]Romanowski, M.C., "Reduced Order Unsteady Aerodynamic and Aeroelastic Models Using Karhunen-Loève Eigenmodes," AIAA-96-3981,1996.
[4]Glauser, M.N., et al., "POD Based Experimental Flow Control on a NACA-4412 Airfoil (Invited)," AIAA-2004-0575.
[5]Lucia, D.J., Beran, P.S., and Silva, W.A., "Reduced-Order Modeling: New Approaches for Computational Physics," *Progress in Aerospace Sciences* 40: 51-117, 2004.
[6]Bui-Thanh, T., Damodaran, M. and Willcox, K., "Proper Orthogonal Decomposition Extensions for Parametric Applications in Transonic Aerodynamics", AIAA Paper 2003-4213, presented at 15th Computational Fluid Dynamics Conference, Orlando, FL, June 2003.
[7]LeGresley, P.A., Alonso, J.J., "Airfoil Design Optimization Using Reduced Order Models Based on Proper Orthogonal Decomposition," AIAA-2000-2545, 2000.
[8]Everson, R. and Sirovich, L. "Karhunen-Loève Procedure for Gappy Data," *J. Opt. Soc. Am. A*, Vol.12, No.8, 1657, 1995.
[9]Sirovich, L. "Turbulence and the Dynamics of Coherent Structures." *Quarterly of Applied Mathematics*, 45: 561-571, 1987.
[10]Hicks, R.M. and Henne, P.A., "Wing Design by Numerical Optimization," *Journal of Aircraft*, 15:407-412, 1978.
[11]AEROFLO Multi-Disciplinary Software User Guide, Thaerocomp Technical Corporation. Nov. 2004.

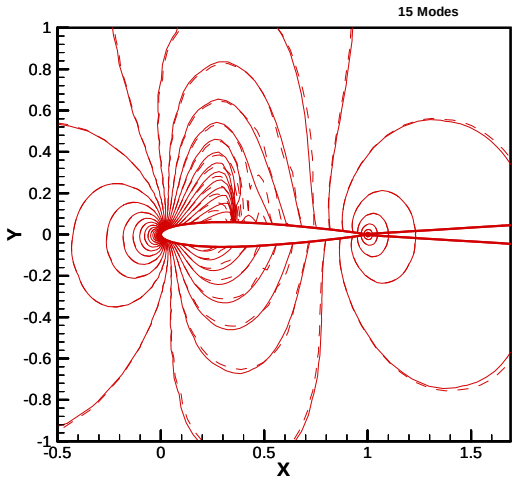

Figure 1(a): Reconstruction of the pressure field by the Gappy POD method (dashed) compared to the original CFD results (solid) (5 POD modes)

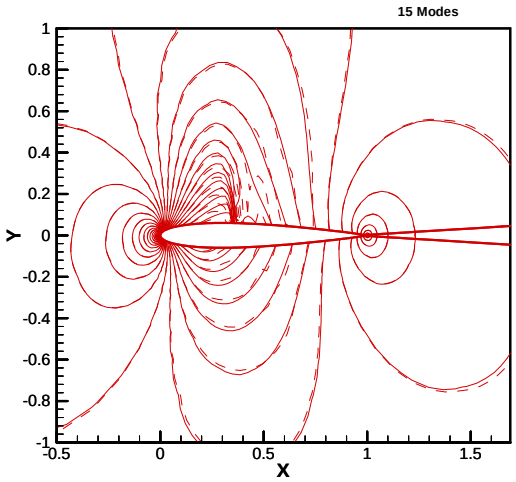

Figure 1(b): Reconstruction of the pressure field by the Gappy POD method (dashed) compared to the original CFD results (solid) (15 POD modes)

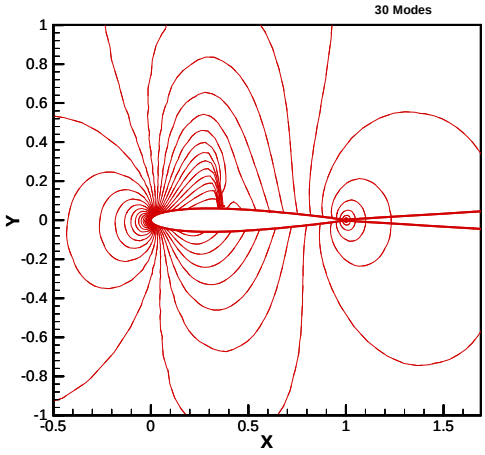

Figure 1(c): Reconstruction of the pressure field by the Gappy POD method (dashed) compared to the original CFD results (solid) (with total 30 POD modes)

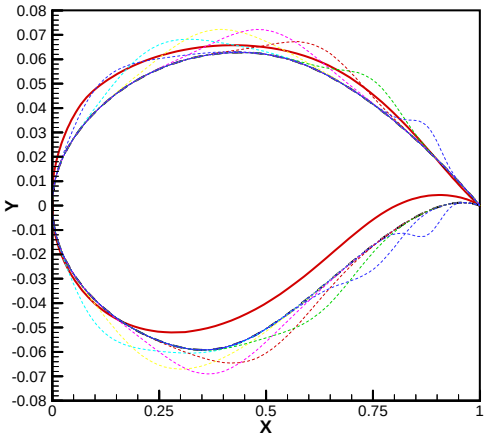

Figure 2: Parameterized airfoils based on RAE 2822 (dash) and the Korn airfoil (solid).

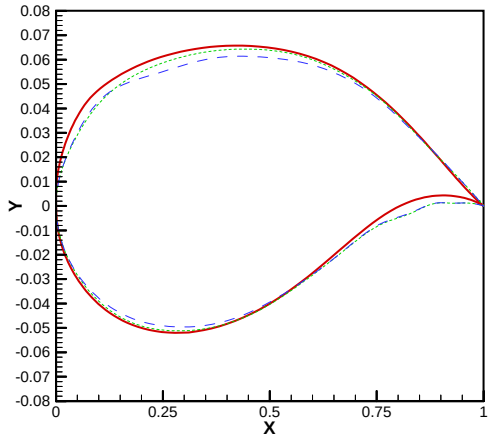

Figure 3(a): Inverse design of the Korn airfoil (solid) using the Gappy POD method (long dash) and gradient-based optimization (short dash). 15 snapshots.

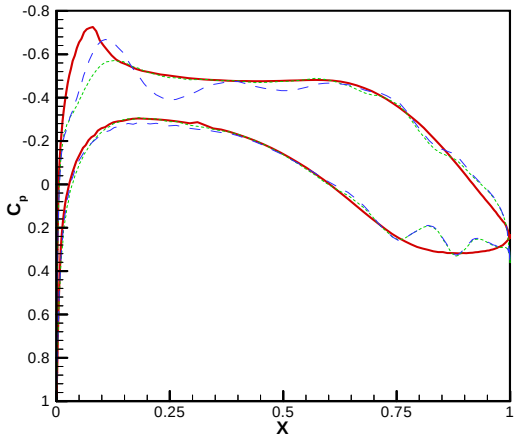

Figure 3(b): Designed surface pressure distributions using the Gappy POD method (long dash) and gradient-based optimization (short dash), compared to the target (solid). 15 snapshopts.

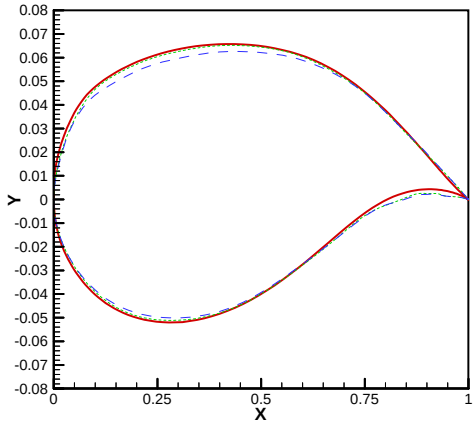

Figure 3(c): Inverse design of the Korn airfoil (solid) using the Gappy POD method (long dash) and gradient-based optimization (short dash). 20 snapshots.

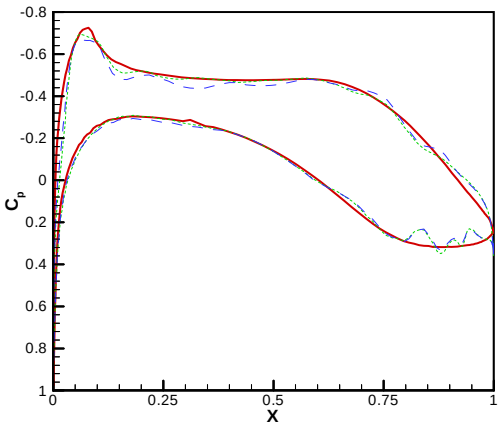

Figure 3(d): Designed surface pressure distribution using the Gappy POD method (long dash) and gradient-based optimization (short dash), compared to the target (solid). 20 snapshots

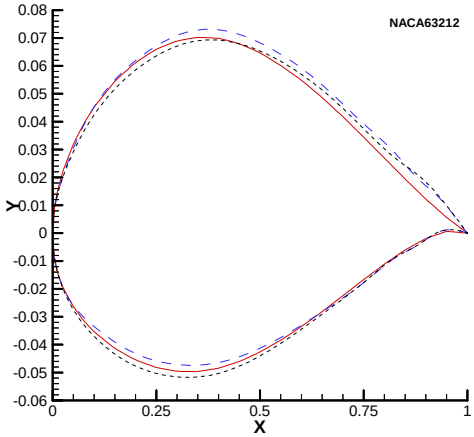

Figure 4(a): Inverse design of the NACA63212 airfoil (solid) using the Gappy POD method (long dash) and gradient-based optimization (short dash). 15 snapshots.

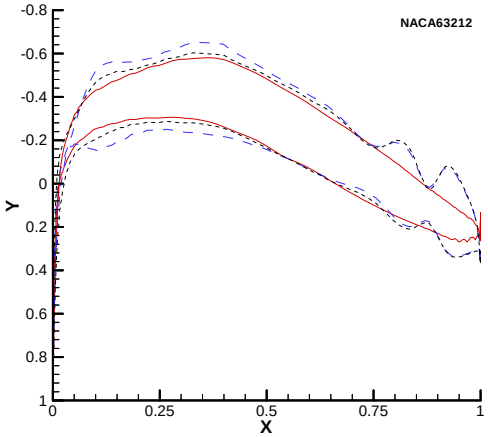

Figure 4(b): Designed surface pressure distributions using the Gappy POD method (long dash) and gradient-based optimization (short dash), compared to the target (solid). 15 snapshots.

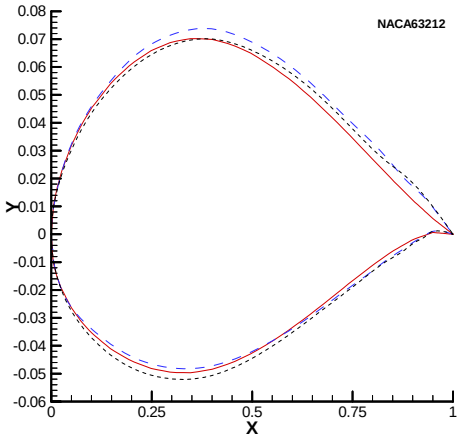

Figure 4(c): Inverse design of the NACA63212 airfoil (solid) using the Gappy POD method (long dash) and gradient-based optimization (short dash). 20 snapshots.

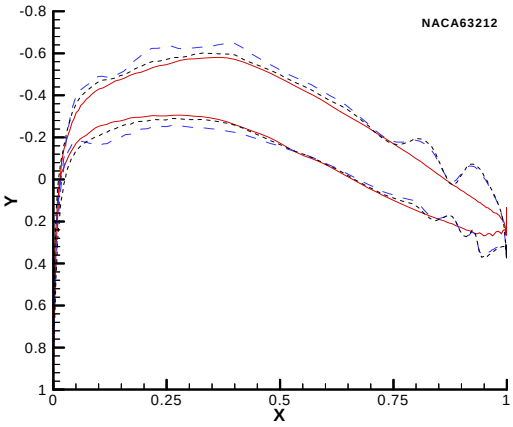

Figure 4(d): Designed surface pressure distributions using the Gappy POD method (long dash) and gradient-based optimization (short dash), compared to the target (solid). 20 snapshots.

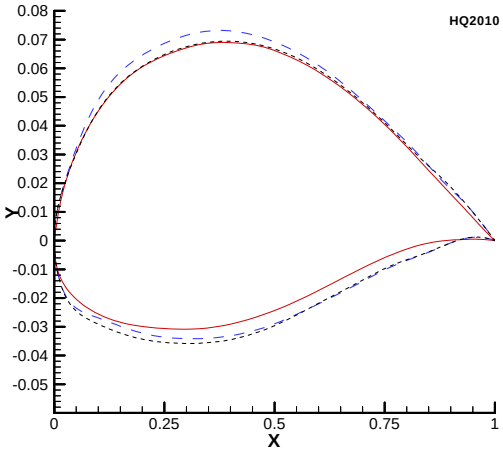

Figure 5(a): Inverse design of the HQ2010 airfoil (solid) using the Gappy POD method (long dash) and gradient-based optimization (short dash). 15 snapshots.

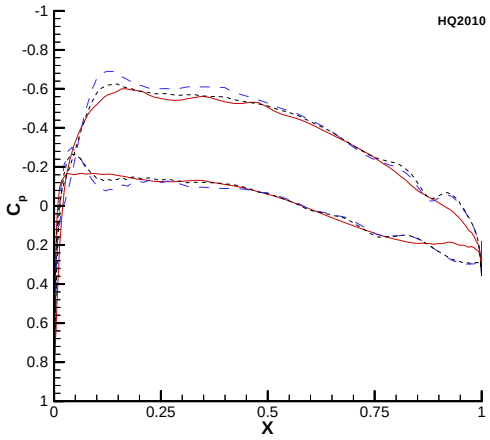

Figure 5(b): Designed surface pressure distributions using the Gappy POD method (long dash) and gradient-based optimization (short dash), compared to the target (solid). 15 snapshots.

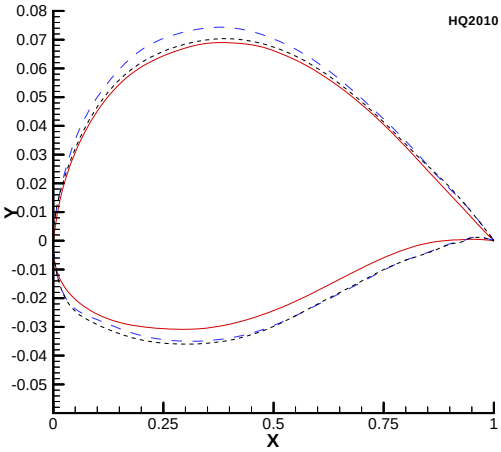

Figure 5(c): Inverse design of the HQ2010 airfoil (solid) using the Gappy POD method (long dash) and gradient-based optimization (short dash). 20 snapshots.

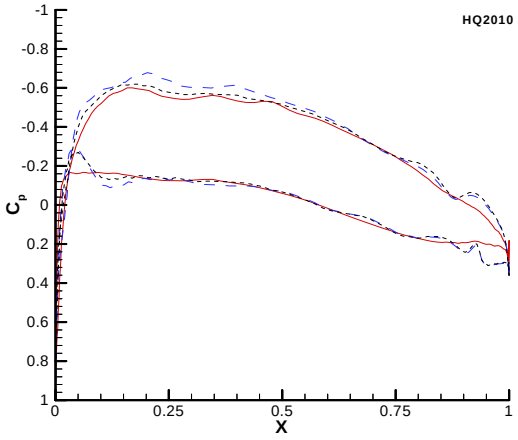

Figure 5(d): Designed surface pressure distribution using the Gappy POD method (long dash) and gradient-based optimization (short dash), compared to the target (solid). 20 snapshots.

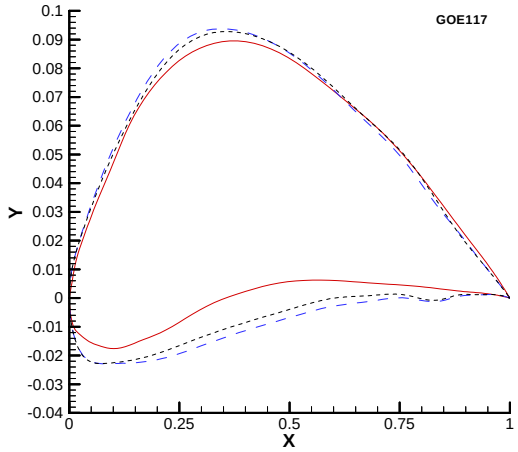

Figure 6(a): Inverse design of the GOE117 airfoil (solid) using the Gappy POD method (long dash) and gradient-based optimization (short dash). 15 snapshots.

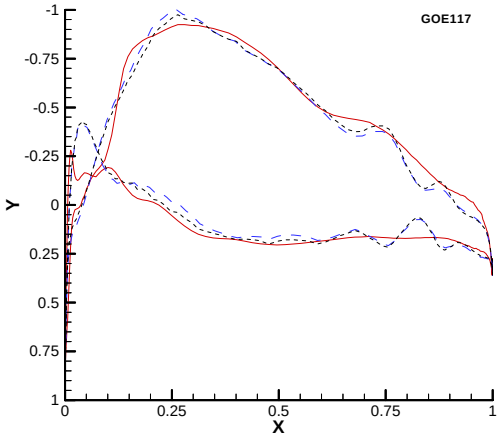

Figure 6(b): Designed surface pressure distributions using the Gappy POD method (long dash) and gradient-based optimization (short dash), compared to the target (solid). 15 snapshopts.

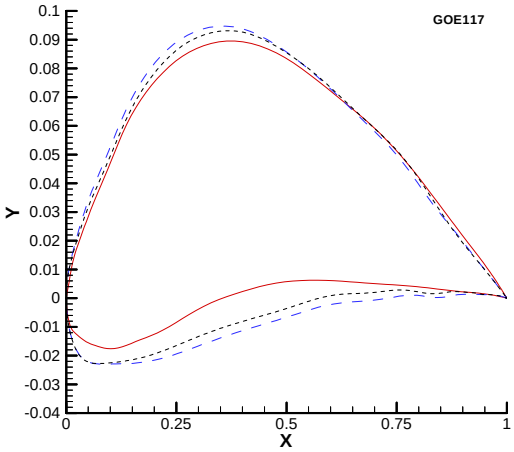

Figure 6(c): Inverse design of the GOE117 airfoil (solid) using the Gappy POD method (long dash) and gradient-based optimization (short dash). 20 snapshots.

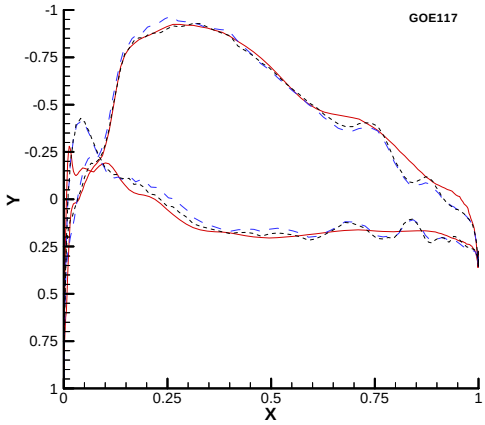

Figure 6(d): Designed surface pressure distribution using the Gappy POD method (long dash) and gradient-based optimization (short dash), compared to the target (solid). 20 snapshots